Maskless direct growth of carbon nanotube micropatterns on metallic substrates

*Olli Pitkänen,[1] Amelia H. C. Hart,[2] Robert Vajtai, [*2] Pulickel M. Ajayan,[2] Krisztian Kordas[1*]*

1 Microelectronics Research Unit, Faculty of Information Technology and Electrical Engineering, University of Oulu, P.O. Box 4500, FIN-90014 University of Oulu, Finland

2 Department of Material Science and NanoEngineering, Rice University, Houston, Texas 77005, United States

ABSTRACT: Herein, we report on a simple process, which is suitable for producing carbon nanotube micropatterns on steel alloys without using any catalyst deposition. The method is based on a pulsed laser beam induced surface microstructuring followed by a thermal chemical vapor deposition growth of carbon nanotubes that emerge exclusively from the surface areas previously exposed to the laser pulses. As concluded from X-ray diffraction, electron microscopy, Raman and X-ray photoelectron spectroscopy analyses of pristine and laser treated surfaces, the area-selective growth is caused by a formation of a thin and nanostructured metal oxide layer during the laser treatment, which is then partially reduced during the subsequent nanotube growth steps. The partially reduced oxide nanoparticles provide catalytic sites for nanotube growth and also believed to disable diffusion of catalytic metal atoms to the subsurface regions giving rise to stable catalyst nanoparticle formation and nanotube growth in the chemical vapor deposition step. The proposed method is fast, scalable and can pave the road for applications, which demand close metal to nanotube contacts with arbitrary microscopic pattern definition on two and three-dimensional

surfaces such as those used in electromechanical contacts, electrochemical electrodes, field emitters, thermal interfaces among many others.

1. Introduction

While a number of different methods exist to synthesize carbon nanotubes (CNTs) including laser ablation,[1-3] arc discharge[4-6] and chemical vapor deposition,[7,8] only the latter technique is known to be suitable for patterned growth by applying multi-step lithography defined templates.[9,10] Two types of processes are applied to accomplish such. In the first, a micropattern of catalyst nanoparticles (Fe, Co, Ni and their combinations) is deposited on a chemically inert support (e.g., SiO_2, Al_2O_3) to avoid diffusion and reaction of the catalyst metal while synthesizing the CNTs.[11] In the second type of process, the surface is micropatterned in a way that certain areas are reactive for the subsequently deposited catalyst thus poisoning the metal (e.g., Si and Au substrates, which form metal silicides and intermetallics, respectively) at the high CNT synthesis temperatures, whereas other parts of the template, on which CNTs are intended to be grown are inert (e.g. SiO_2, Al_2O_3).[12] Alternatively, one may also apply micropatterns of thin Ti and Al films as relatively stable support for the catalyst, since these metals oxidize rapidly when exposed to air and the formed oxide can already act as a diffusion barrier.[13,14] Interestingly, some aluminum[15] and steel[16-19] alloys were also found as suitable supports for catalysts in CNT growth, which is likely caused by superficial oxides on the surface that inhibit the rapid diffusion and dissolution of the added catalyst nanoparticles thus contributing to their reasonably long lifetime and active presence for CNT growth. Oxidation and subsequent reduction of steel surfaces at elevated temperatures has been reported to be an efficient way to make the surface particularly active for the CVD growth process even without depositing additional catalyst on the surface.[20-23] However, patterned growth on these alloys have not been reported yet.

In our current study, an innovative approach is proposed to achieve patterned growth of CNTs on steel alloys by the means of localized area-selective activation using short laser pulses. Surface parts affected

by the laser pulses are shown to undergo oxidation, which become partially reduced upon the high temperature CVD process. As a consequence, due to the presence of both barrier-type oxide and catalytic metal phases, the illuminated areas facilitate highly active sites for CNT growth without adding any catalyst before or during the chemical vapor growth thus significantly simplifying the overall process.

2. Results and discussion

The laser processed regions of the surfaces of the metallic substrates undergo visible changes as displayed in the scanning electron micrographs (Fig. 1a-c and Fig. S1). Formation of nanoscopic cracks, melted and re-solidified surface features as well as nanostructured particles are observed. The bright contrast of these latter ones indicates electrostatic charging and suggests some kind of superficial oxide phases. Elemental analysis by the means of energy-dispersive X-ray spectroscopy of the pristine and laser treated surface areas show a significant increase of oxygen concentration after laser patterning (Fig. S2 and Fig. S3 a). The CNTs grown on the laser patterned regions of Inconel® are multi-walled and their properties depend on the applied laser power and CVD growth parameters. We found that – in both of the applied CVD methods - the surface density of nanotubes is higher on the substrates which were treated with higher laser powers in the studied parameter range (Fig. 3 d-f), accordingly we did not treat substrates with lower power; and we did not extend the laser power higher as the surface roughness increased in those cases to the level when micropatterning lost its purpose. In the CVD processes one of the key factors is to provide the catalytic metallic particles by reduction of the oxide phases, we applied ammonia or hydrogen as the reducing agent. In case of H_2, the reduction happens in the same step with the carbon deposition, while in case of NH_3, a weaker reducing agent, a longer reaction time was allowed in the form of pre-treatment as it is described in the Experimental methods. The CVD process using NH_3 annealing provided better selectivity than the one carried out with H_2 carrier gas (Fig. S4), however the abundance and length of the nanotubes were larger in the H_2 based process. The nanotubes grown with the NH_3 annealing process have an average diameter of ~20 nm (Fig. S3 b), Raman I_D/I_G -peak ratio of 0.65 (Fig.

S3 c) and length of up to a few micrometers (Fig. S5 a) with some occasional inner carbon wall in the inner structure of larger tubes (Fig. S5 b). With H_2 synthesis the nanotubes have an average diameter of ~10 nm (Fig. S3 b), Raman I_D/I_G -peak ratio of 0.85 (Fig S3 c), and length of a few tens of micrometers (Fig. S5 c) with less occurrence of inner tube walls (Fig. S5 d). Interestingly the CNTs synthesized with NH_3 had lower I_D/I_G -peak ratio suggesting having lower amount of defects in their lattice although the synthesis temperature (600 °C) is lower compared to the H_2 assisted synthesis (660 °C). The selectivity of growth on Inconel® 600 is illustrated in Fig. 1 g-j showing a bitmap raster pattern, in which the dark pixels represent the laser processed and subsequently CNT populated surface regions. CNT growth on laser processed AISI 304ss stainless steel substrate was much poorer (Fig. S6).

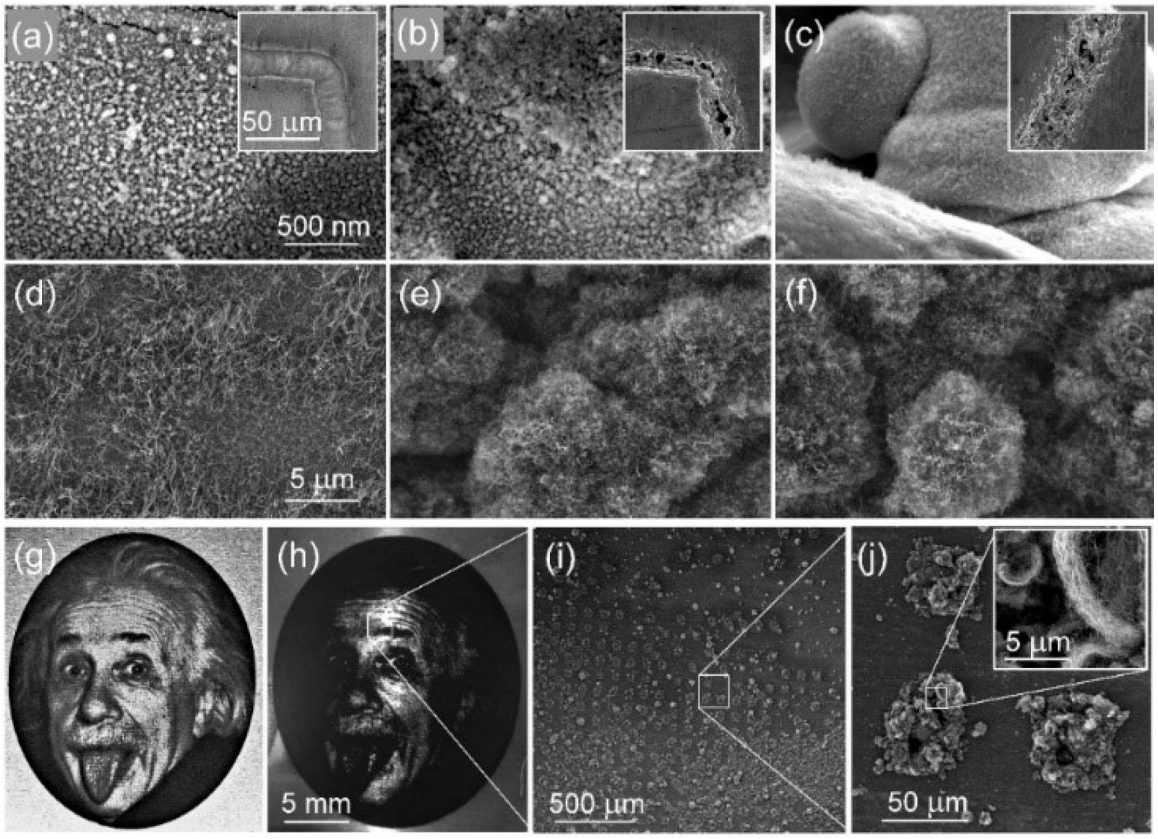

Figure 1 Close-up SEM images of laser processed Inconel® 600 surfaces using scanned laser pulses of total average power of (a) 1.3 W (b) 2.1 W and (c) 3.2 W. Low magnification SEM images in the insets display the corresponding micropatterns. Panels (d), (e) and (f) show CNT forests grown on the corre-

sponding laser patterned areas. CNT synthesis was carried out at 550 °C using the NH_3 annealing synthesis. (g) Digital camera pictures of a bitmap raster image (2 bit) of Albert Einstein patterned on the Inconel 600® substrate. (h) Chemical vapor deposition of CNTs on a laser micropatterned Inconel® 600 surface similar to that in the previous panel. Growth was done in H_2 based method at 670 °C. Panels (i) and (j) show the image pixels (50×50 μm^2) in different SEM magnifications. Inset in panel (j) is a close-up of CNT bundles in a single pixel.

Laser-assisted rapid heating and subsequent cooling of steels alloys is known to yield hardening of the surface as a consequence of formed fine grain structure and dislocations as well as residual compressive stresses in the superficial heat affected zones.[24-26] In AISI 304ss steel, like our test surfaces besides Inconel® 600, laser shock peening was reported to induce a nanocrystalline structure, twinings as well as deformation induced martensite formation,[24] in an excellent agreement with our X-ray diffraction measurements on AISI 304ss steel (Fig. 2a).The residual compressive stress of several hundreds of MPa reported after laser shock peening[25] gives a reasonable explanation of the positive 2Θ shift of the diffraction peeks in our Inconel® 600 and AISI 304ss steel samples. The shift of 0.3˚ for the austenitic (111) reflection indicates a strain of 0.0067, which corresponds to a compressive stress of ~1300 MPa considering an elastic modulus E_{304} = 200 GPa of AISI 304ss steel. For Inconel® 600, the shift is 0.25˚ due to a compressive strain of 0.0053 caused by a residual stress of 1100 MPa (E_{600} = 214 GPa). Further, the appearance of the additional reflection at 44.6˚ in the case of the steel surface is a signature of the partial martensitic transformation and can be indexed with the (110) plane. On the other hand, new reflections in the case of laser annealed Inconel® 600 were not observed, i.e. the structure remains austenite, in good agreement with another report on resolidified surfaces after laser-melting.[26]

In previous studies, growth of CNTs of various industrial steel alloys has been concluded to be a consequence of nanostructures of catalytically active surface features[27] as well as surface enriched chromium oxides through which iron can diffuse and act as a catalyst for the nanotube synthesis.[28] The combination of thermal annealing and plasma ion bombardment of Inconel® 600 metal and austenitic stainless steel

(SUS316L) substrates has been reported to cause nanoparticle structure formation and enhance growth of carbon nanotubes on such surfaces.[29,30] Since we do not observe any crystalline oxide phases in the X-ray diffraction patterns neither before nor after laser processing, we extended our analyses using Raman spectroscopy (Fig. 2b).

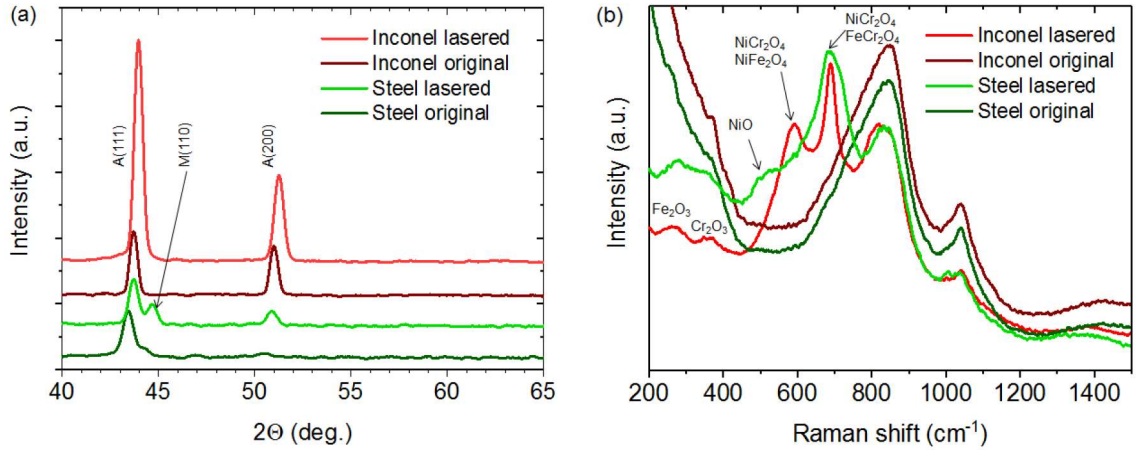

Figure 2 (a) Raman spectra and (b) X-ray diffraction patterns of the original and laser-processed steel and Inconel® alloy 600 surfaces. The laser parameters were 1900 mW power at 40 kHz pulse repetition with 5 mm/s scanning speed.

Raman spectra acquired before and after laser processing of our alloys show the formation of various oxide phases on the surface. In the case of AISI 304ss steel, three new Raman peaks emerge at around 500, 670 and 690 cm^{-1}, which can be assigned to NiO (510 cm^{-1}), Fe_3O_4 (670 cm^{-1}), $FeCr_2O_4$ (686 cm^{-1}) and $NiCr_2O_4$ (686 cm^{-1})[31] For Inconel® 600, we observe two new peaks at around 580 cm^{-1} and 680 cm^{-1} that are signatures of $NiCr_2O_4$ (580 cm^{-1}), $NiFe_2O_4$ (595 cm^{-1}) as well as the already identified Fe_3O_4 (670 cm^{-1}), $FeCr_2O_4$ (686 cm^{-1}) or $NiCr_2O_4$ (686 cm^{-1}) phases.[31] It is worth pointing out that the broad Raman band below 450 cm^{-1} caused by surface oxyhydroxydes of iron (γ-FeOOH at 250 cm^{-1} and α-FeOOH at 390 cm^{-1}) are vanished after laser processing, whereas some minor oxide peaks assigned to Fe_2O_3 (220 cm^{-1}) and Cr_2O_3 (351 cm^{-1}) appear in the spectra.[32] These findings support well the presence of nanostructured poorly conductive layers observed by SEM and explain the increased oxygen concentration measured by EDX in the laser pattered regions.

In the light of previous reports and our current XRD, Raman and EDX analyses, we may conclude that the favored growth of CNTs along the laser patterned areas of Inconel® 600 and AISI 304ss steel samples is a result of multiple events. Firstly, the rapid heating, melting and re-solidification of the alloys yield fine nanostructured grains. Secondly, superficial oxide layer formation takes place due to the very high surface temperature (above 1000 ˚C) localized in the laser processed region (in the heat-affected zone). Thirdly, as it can be seen in XPS analysis of the substrates reduced in the process conditions without carbon precursor (Fig. 3 and Fig. S7), the surface oxides undergo a partial reduction when exposed to the highly reductive carrier gases (H_2 or NH_3) at the CVD growth temperature (660 °C or 600 °C respectively) and the as formed catalytic metals are in close contact with some residual non-reduced oxide acting as support and diffusion barrier. In Ni 2p spectra (Fig 3 a) the metallic Ni $2p_{3/2}$ peak at 852.5 eV is getting more dominant after the reduction processes, and the reduction in H_2 conditions appears to be more effective compared to NH_3 conditions. The same tendency is seen in Fe 3p spectra with metallic iron peak at 52.9 eV. (Note that Fe 2p spectra gives stronger signal but it overlaps with Ni LNM auger peaks and therefore it is not the most suitable peak to analyze Inconel® 600.) However it also shows clear increase of metallic Fe $2p_{3/2}$ at 706.9 eV (Fig S7 a) after the reduction. In the Cr 2p spectrum (Fig 3 c) while reduction of CrO_3 (578.9 eV) is the most evident there are still clear CrO_2 and Cr_2O_3 peaks after both types of reduction processes. Interestingly the Cr metal peak (574.1 eV) appears to be the strongest after the NH_3 reduction where chromium nitride peaks can also be fitted, and which is also supported by the N 1s spectra (Fig 3 d and Table S1) displaying CrN at 369.2 eV and Cr_2N at 396.7 eV. The slight peak shift compared to the literature is likely caused by interstitial nitrogen atoms at 398.4 eV.[33] Our findings in the Ni 2p, Fe 3p and Cr 2p spectra are supported by O 1s spectra (Fig S7 b) that indicate more pronounced reduction of Ni and Fe oxides (at ~530 eV) than that of Cr (III) and Cr (IV) oxides (at ~531 eV).[34]

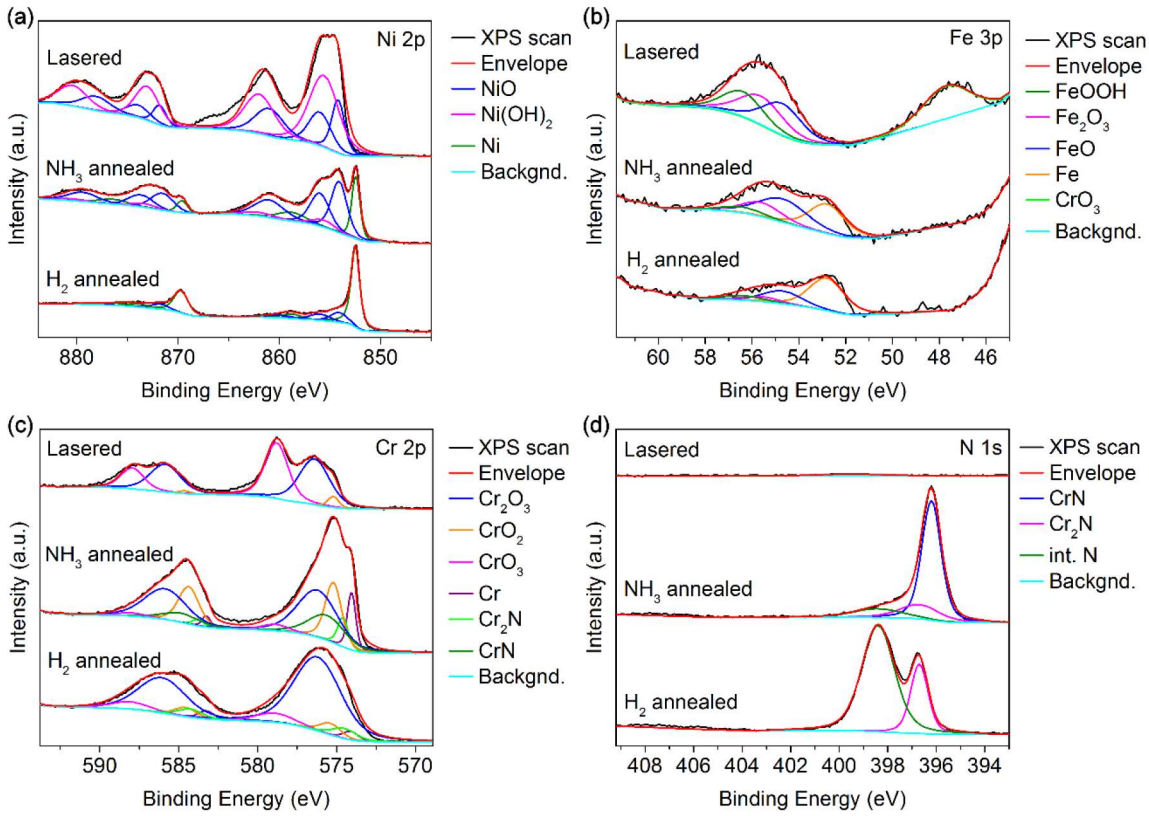

Figure 3 XPS data and fitted peaks measured from (a) Ni 2p, (b) Fe 3p, (c) Cr 2p and (d) N 1s spectral area measured from Inconel® 600 substrates after laser process and subsequent anneal processes in NH_3 or H_2. The laser parameters were 2100 mW power at 60 kHz pulse repetition with 5 mm/s scanning speed.

STEM imaging and EDX element maps from the substrate-CNT interface grown using NH_3 process (Fig 4 a) show that surface layer is enriched in Cr, O and N (i.e. oxides and nitrides of chromium), whereas the nanoscopic plugs at the bottom the nanotubes are composed of Ni and Fe as a result of the reductive reaction conditions during CNT synthesis. These alloyed nanoparticles of Ni and Fe on the top of chromium oxides act as catalyst for base grown CNTs (Fig 4 b). TEM images of the tips of CNTs (Fig S8) displaying the absence of catalyst also support the base growth mechanism. Our findings are coherent with the generally accepted vapor-liquid-solid (VLS) growth model, which necessitates the presence of a catalyst for the growth of CNTs. In addition, as the growth takes place on a solid template at elevated temperatures, the catalyst nanoparticles need stabilization, which is provided by surface oxides that inhibit (or at least retard) the diffusion of the catalyst alloys into the bulk of the substrate.[27-30]

It is worth pointing out here, that previous studies reporting on CNTs grown on steels without additional catalyst apply pretreatments such as (i) etching with HCl followed by thermal oxidation,[27] (ii) surface polishing, acid etching and subsequent oxidation as well as reduction,[20] (iii) thermal oxidation and reduction,[21,23,28] and (iv) air annealing and plasma treatments.[29,30] While each method has its own peculiar consequence on the surface morphology/topology, chemical composition and thus CNT growth, the common feature is the formation of superficial diffusion barrier oxides and adjacent catalytic metal and alloy nanoparticles, which is similar to our process.

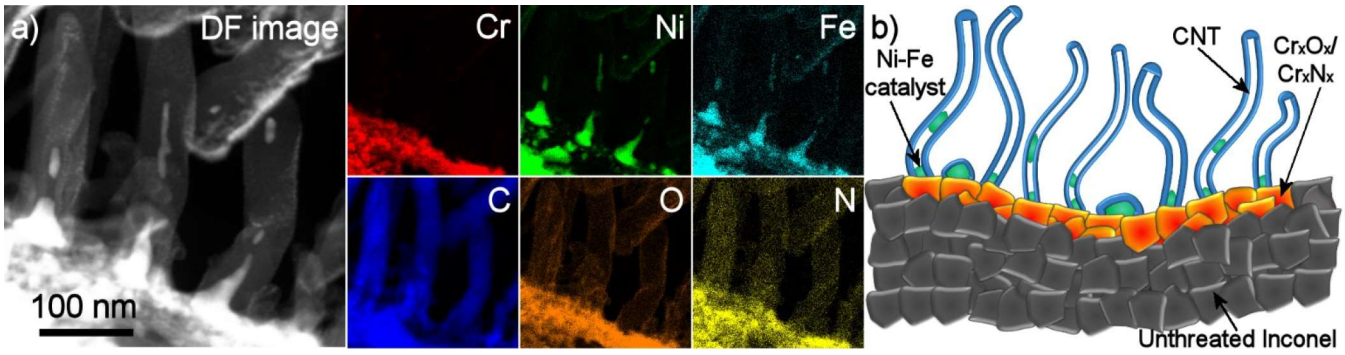

Figure 4 (a) Dark-field STEM and EDX elemental mapping (Cr, Ni, Fe, C, O and N) images of the metal substrate-CNT interface of a sample grown using NH_3 anneal at 600 °C on Inconel® 600. (b) Illustration of the substrate-CNT interface.

3. Conclusions

In conclusion, we have shown an additive method to produce micropatterned CNT films is not only maskless but also avoids using added catalyst. The selective growth of carbon nanotubes on the laser annealed surface parts is due to the surface oxidation (during the laser processing) and subsequent partial reduction (during CNT growth) of the surface, which create a unique catalytic surface layer on the substrate with Fe and Ni nanoparticles supported by Cr oxides and nitrides. The process is rapid and easy to scale up as it involves only two steps, laser activation and chemical vapor deposition and thus avoids tedious multi-step lithography. We expect that the process may be improved further to get better pattern definition by using laser beams with smaller focal spot diameter and shorter duration. We also envisage

potential for patterned CNT growth on 3-dimensional metal surfaces. Further, as the carbon nanotubes are directly grown on metallic substrates, direct metal-CNT contacts form, which prompts applications in electrochemical sensors,[35] and energy conversion[36] and storage,[12] as well as electromechanical contacts and switches,[37] and thermal management[38] that are accomplished today either by lithographically defined templates or by post-mounted CNT architectures.

4. Methods

Laser processing of the growth substrates: The metal sheets (Inconel 600®, thickness of 200 μm, Goodfellow and AISI 304ss stainless steel, thickness of 150 μm) were cut and patterned using Siemens Microbeam 3200 (3ω Nd:YVO_4, λ=355 nm, τ~20 ns, ~20 μm focal spot diameter) and LPKF ProtoLaser U3 (Nd:YVO_4, λ=355 nm, τ~20 ns, ~20 μm focal spot diameter) pulsed laser systems with average laser powers ranging from 1.3 W to 3.2 W and laser repetition rates between 20 kHz and 100 kHz. The metal samples were washed with acetone and dried before the laser processing carried out in ambient air.

CNT synthesis was carried out using a cold-walled chemical vapor deposition reactor equipped with 2" graphite heater (Aixtron Black Magic 2"). Two different synthesis approaches were applied. In the first method, the samples were heated to 550 or 600 °C and annealed in NH_3 flow (250 sccm, 10 mbar) for 10 minutes, the chamber was then evacuated into 0.2 mbar base pressure after which it was filled back to 10 mbar pressure of N_2 and 250 sccm flow was maintained. After the process pressure was stabilized, carbon precursor (C_2H_2, 25 sccm) was introduced to the chamber for 10 minutes to enable the CNT synthesis. In the second method, the chamber was first filled to 500 mbar applying gas flows of 700 sccm H_2, 500 sccm N_2 and 10 sccm C_2H_2 and after the target pressure was reached the sample was heated to 660 or 670 °C for 10 minutes.

Analyses: The structure and chemical composition of the materials were studied with field emission scanning electron microscopy (FESEM, Zeiss Ultra Plus and Oxford Instruments EDX detector installed on the device), transmission electron microscopy (TEM, JEOL JEM-2200FS EFTEM/STEM 200 kV), X-

ray diffraction (XRD, Bruker D8 Discover, Cu Kα -radiation) and Raman spectroscopy (Horiba Jobin-Yvon LabRAM HR800 UV-vis μ-Raman, λ=488 nm). In X-ray photoelectron spectroscopy (XPS, Thermo Fisher Scientific Escalab 250 XI system with Al Kα X-ray source, 1486.6 eV, data evaluation using Avantage software) analysis the samples were first analyzed after the laser process and were then annealed in the corresponding H_2 and NH_3 environments without the carbon precursor for 10 minutes. The samples were then transferred for the second analysis in desiccators with N_2 atmosphere. The cross section sample of the metal substrate - CNT interface was prepared with Focused Ion Beam (FIB, FEI Helios DualBeam), for STEM EDX element mapping analysis.

ASSOCIATED CONTENT

Supporting Information. Element concentration of substrates before and after laser processing; CNT diameter histograms, Raman spectra as well as additional SEM and TEM images; X-ray photoelectron spectra of substrates after various process conditions are displayed in the Supporting information.

AUTHOR INFORMATION

Corresponding Authors

*Krisztian Kordas, krisztian.kordas@oulu.fi and Robert Vajtai, robert.vajtai@rice.edu

ACKNOWLEDGMENT

We acknowledge the support received from the Micro- and Nanotechnology Center, University of Oulu. O.P. acknowledges Tauno Tönning foundation, Ulla Tuominen foundation, Riitta and Jorma J. Takanen foundation and Finnish Foundation for Technology Promotion for their support.

REFERENCES

1. Scott, C.D.; Arepalli, S.; Nikolaev, P.; Smalley, R.E. Growth mechanisms for single-wall carbon nanotubes in a laser-ablation process. *Appl. Phys. A* **2001**, *72*, 573–580.

2. Guo, T.; Nikolaev, P.; Thess, A.; Colbert, D.T.; Smalley, R.E. Catalytic growth of single-walled manotubes by laser vaporization. *Chem. Phys. Lett.* **1995**, *243*, 49-54.

3. Thess, R. Lee, P. Nikolaev, H. Dai, P. Petit, J. Robert, C. Xu, Y.H. Lee, S.G. Kim, A.G. Rinzler, D.T. Colbert, G.E. Scuseria, D. Tomanek, J.E. Fischer, R.E. Smalley: Crystalline Ropes of Metallic Carbon Nanotubes. *Science* **1996**, *273*, 483-487.

4. Journet, C; Maser, W.K.; Bernier, P.; Loiseau, A.; delaChapelle, M.L.; Lefrant, S.; Deniard, P.; Lee, R.; Fischer, J.E., Large-scale production of single-walled carbon nanotubes by the electric-arc technique. *Nature* **1997**, *388* 756-758.

5. Bethune, D.S.; Kiang, C.H.; Devries, M.S.; Gorman, G.; Savoy, R.; Vazquez, J.; Beyers, R.; Cobalt-catalyzed growth of carbon nanotubes with single-atomic-layer walls. *Nature* **1993**, *363*, 605-607.

6. Ebbesen, T.W.; Ajayan, P.M. Large-scale synthesis of carbon nanotubes, *Nature*, **1992**, *358*, 220-222

7. Amelinckx, S.; Zhang, X. B.; Bernaerts, D.; Zhang, X. F.; Ivanov, V.; Nagy, J. B. A formation mechanism for catalytically grown helix-shaped graphite nanotubes. *Science* **1994**, *265*, 635–639.

8. Endo, M.; Takeuchi, K.; Kobori, K.; Takahashi, K.; Kroto, H.W.; Sarkar, A. Pyrolytic carbon nanotubes from vapor-grown carbon fibres. *Carbon* **1995**, *33*, 873–881.

9. Zhang, ZJ; Wei, BQ; Ramanath, G; Ajayan, PM, Substrate-site selective growth of aligned carbon nanotubes *Appl. Phys. Lett.* **2000**, *77*, 3764-3766.

10. Wei, B. Q.; Vajtai, R.; Jung, Y.; Ward, J.; Zhang, R.; Ramanath, G.; Ajayan, P. M. Organized assembly of carbon nanotubes. *Nature* **2002**, *416*, 495-496

11. Mattevi, C.; Wirth, C. T.; Hofmann, S; Blume, R.; Cantoro, M.; Ducati, C.; Cepek, C.; Knop-Gericke, A.; Milne, S.; Castellarin-Cudia, C.; Dolafi, S.; Goldoni, A.; Schloeg, R.; Robertson, J. In-situ X-ray Photoelectron Spectroscopy Study of Catalyst−Support Interactions and Growth of Carbon Nanotube Forests. *J. Phys. Chem. C* **2008**, *112* 12207–12213.

12. Halonen, N.; Kordás, K.; Tóth, G.; Mustonen, T.; Mäklin, J.; Vähäkangas, J.; Ajayan, P. M.; Vajtai, R. Controlled CCVD synthesis of robust multi-walled carbon nanotube films, *J. Phys. Chem. C* **2008**, *112,* 6723.

13. Pitkänen, O.; Lorite, G.S.; Shi, G.; Rautio, A.-R.; Uusimäki, A.; Vajtai, R.; Tóth, G.; Kordás, K. The effect of Al buffer layer on the catalytic synthesis of carbon nanotube forests, *Top. Catal.* **2015**, *58*, 1112-1118.

14. Pitkänen, O.; Järvinen, T.; Cheng, H.; Lorite, G. S.; Dombovari, A.; Rieppo, L.; Duong, H.M.; Talapatra, S.; Tóth, G.; Juhasz, K. L.; Konya, Z.; Kukovecz, A.; Ajayan, P.M.; Vajtai, R. Kordás, K. On-Chip integrated vertically aligned super and pseudocapacitors. *Sci. Rep.* **2017**, *7* 16594.

15. Gao, Z.; Zhang, K.; Yuen, M. M. F. Fabrication of Carbon Nanotube Thermal Interface Material on Aluminium Alloy Substrates, 2010 11th International Conference on Electronic Packaging Technology & High Density Packaging, Xi'an, China, pp. 1402-1408.

16. Talapatra, S.; Kar, S.; Pal, S.K.; Vajtai, R.; Ci, L.; Victor, P.; Shaijumon, M.M.; Kaur, S.; Nalamasu, O.; Ajayan, P.M. Direct growth of aligned carbon nanotubes on bulk metals. *Nat. Nanotechnol.* **2006**, *1*, 112-116.

17. Sridhar, S.; Tiwary, C.; Vinod, S.; Taha-Tijerina, J.J.; Sridhar, S.; Kalaga, K.; Sirota, B.; Hart, A.H.C.; Ozden, S.; Sinha, R.K.; Harsh, Vajtai, R.; Choi, W.; Kordás, K.; Ajayan, P.M. Field emission with ultralow turn on voltage from metal decorated carbon nanotubes, *ACS Nano*, **2014**, *8*, 7763–7770.

18. Parthangal, P. M.; Cavicchi, R.e.; Zachariah, M. R. A generic process of growing aligned carbon nanotube arrays on metals and metal alloys. *Nanotechnol.* **2007**, *18*, 185605.

19. Vilatela, J. J.; Rabanal, M. E.; Cervantes-Sodi, F.; García-Ruiz, M.; Jiménez-Rodríguez J. A.; Reiband, G.; Terrones, M. A Spray Pyrolysis Method to Grow Carbon Nanotubes on Carbon Fibres, Steel and Ceramic Bricks. *J. Nanosci. Nanotechnol.* **2015**, *15*, 2858-2864.

20. Hashempour, M.; Vicenzo, A.; Zhao, Fu.; Bestetti, M. Direct growth of MWCNTs on 316 stainless steel by chemical vapor deposition: Effect of surface nano-features on CNT growth and structure. *Carbon* **2013**, *63*, 330-347.

21. Wang, Y.; Li, D.; Sun, W.; Sun, J.; Li, G.; Zhang, H.; Xi, Z.; Pei, X.; Li, Y.; Cheng, Y. Synthesis and field electron emission properties of multi-walled carbon nanotube films directly grown on catalytic stain-less steel substrate, *Vacuum* **2018**, *149*, 195-199.

22. Yamagiwa, K.; Ayato, Y.; Kuwano, J. Liquid-phase synthesis of highly aligned carbon nanotubes on preheated stainless steel substrates. *Carbon* **2016**, *98,* 225-231.

23. Pattinson, S. W.; Viswanath, B.; Zakharov, D. N.; Li, J.; Stach, E. A.; Hart, A. J. Mechanism and Enhanced Yield of Carbon Nanotube Growth on Stainless Steel by Oxygen-Induced Surface Reconstruction. *Chem. Mater.* **2015**, *27*, 932−937.

24. Zhou, L.; He, W.; Luo, S.; Long, C.; Wang, C.; Nie, X.; He, G.; Shen, X.J.; Li, Y. Laser shock peening induced surface nanocrystallization and martensite transformation in austenitic stainless steel, *J. Alloy Compound.* 2016, *655*, 66-70.

25. Nikitin, I.; Scholtes, B.; Maier, H.J.; Altenberger, I. High temperature fatigue behavior and residual stress stability of laser-shock peened and deep rolled austenitic steel AISI 304, *Scripta Mater.* **2004**, *50*, 1345–1350.

26. Lim, Y.S.; Suh, J.H; KUK, I.H.; KIM, J.S. Microscopic investigation of sensitized Ni-base alloy 600, after laser surface melting, *Metallurg. Mater. Trans. A* **1997**, *28A*, 1223-1231.

27. Baddour, C. E.; Fadlallah, F.; Nasuhoglu, D.; Mitra, R.; Vandsburger, L.; Meunier, J.-L. A simple thermal CVD method for carbon nanotube synthesis on stainless steel 304 without the addition of an external catalyst. *Carbon*, **2008**, *47*, 313-347.

28. Sano, N.; Yamamoto, S.; Tamon, H. Cr as a key factor for direct synthesis of multi-walled carbon nanotubes on industrial alloys, *Chem. Eng. J.* **2014**, *242*, 278–284.

29. Shin, E.-C.; Jeong, G.-H. Enhancement of carbon nanotube growth yield on Inconel 600 substrates through the surface pretreatments combining thermal annealing and plasma ion bombardment, *Curr. Appl. Phys.* **2014**, *14*, 8-12.

30. Shin, E.-C.; Jeong, G.H. Highly efficient carbon nanotube growth on plasma pretreated stainless steel substrates, *Thin Solid Films* **2012**, *521*, 102–106.

31. Hosterman B.D. (2011). Raman Spectroscopic Study of Solid Solution Spinel Oxides, University of Nevada. Las Vegas, Doctoral dissertation (paper 1087).

32. Colomban P (2011). Potential and Drawbacks of Raman (Micro)spectrometry for the Understanding of Iron and Steel Corrosion, New Trends and Developments in Automotive System Engineering, Prof. Marcello Chiaberge (Ed.), ISBN: 978-953-307-517-4, InTech, DOI: 10.5772/13436.

33. Wu, M.-C.; Hiltunen, J.; Sapi, A.; Avila, A.; Larsson, W.; Liao, H.C.; Huuhtanen, M.; Tóth, G.; Shchukarev, A.; Laufer, N.; Kukovecz, A.; Kónya, Z.; Mikkola, J.-P.; Keiski, R.; Su, W.-F.; Jantunen, H.; Kordás, K. Nitrogen-doped TiO_2 anatase nanofibers decorated with noble metal nanoparticles for high-efficiency photocatalytic hydrogen generation. *ACS Nano* **2011**, *5*, 5025-5030.

34. NIST X-ray Photoelectron Spectroscopy Database, (URL: https://srdata.nist.gov/xps/Default.aspx), Visited 2018/01/08

35. Lin, JF; Pitkanen, O; Maklin, J.; Puskas, R.; Kukovecz, A.; Dombovari, A.; Toth, G.; Kordas, K. Synthesis of tungsten carbide and tungsten disulfide on vertically aligned multi-walled carbon nanotube forests and their application as non-Pt electrocatalysts for the hydrogen evolution reaction, *J. Mater. Chem. A*, **2015**, *3*, 14609-14616.

36. Aitola, K.; Halme, J.; Halonen, N.; Kaskela, A.; Toivola, M.; Nasibulin, A.G.; Kordas, K.; Toth, G.; Kauppinen, E.I.; Lund, P.D. Comparison of dye solar cell counter electrodes based on different carbon nanostructures, *This Solid Films* **2011**, *519*, 8125-8134.

37. Toth, G.; Mäklin, J.; Halonen, N.; Palosaari, J.; Juuti, J.; Jantunen, H.; Kordas, K.; Sawyer, W. G.; Vajtai, R.; Ajayan, P.M. Carbon Nanotube Based Electrical Brush Contacts. *Adv. Mater.* **2009**, *21*, 2054-2058.

38. Kordás, K.; Tóth, G.; Moilanen, P.; Kumpumäki, M.; Vähäkangas, J.; Uusimäki, A.; Vajtai, R. Ajayan, P.M. Chip cooling with integrated carbon nanotube microfin architectures. *App. Phys. Lett.* **2007**, *90*, 123105.